River Flow 2006 – Ferreira, Alves, Leal & Cardoso (eds)

Experimental study of bed load on steep slopes

Philippe Frey, Matthieu Dufresne, Tobias Böhm & Magali Jodeau
Cemagref Grenoble, ETNA, Saint Martin d'Hères Cedex, France

Christophe Ancey
Ecole Polytechnique Fédérale de Lausanne, Ecublens, Lausanne, Switzerland

ABSTRACT: An important issue in the study of bed load transport in gravel-bed rivers is related to the physical mechanisms governing the bed resistance and particle motion. In order to better understand the physical processes ruling bed load solid transport at the grain scale, an experimental study of the motion of coarse spherical glass beads entrained by a turbulent and supercritical water flow down a steep channel with a mobile bed was set up. The initial width was 6.5 mm slightly larger than the particle diameter of 6 mm to create a two-dimensional particle flow allowing recording from the side all particles with a high speed camera. The overall aim of this research is to measure the trajectories of all particles and to analyze the fluctuations of the solid discharge as well as the state of movement, rolling or saltation. This paper is focussing on global hydrodynamic and equilibrium solid transport results. The channel inclination ranged from 7.5% to 15% and a doubled width of 12.7 mm was also studied. Data were corrected with the Einstein's method to account for side-wall effects. Non-dimensional solid discharge vs. Shields numbers results are in good agreement with classical incipient motion Shields numbers and compare favorably with two specific semi-empirical bed-load formulae. Those results show that upscaling of data obtained at the particle scale to the reach scale is possible despite the unusual hydraulic configuration of this narrow channel.

1 INTRODUCTION

Despite substantial progress made over the last two decades in the physical understanding of the motion of coarse particles in a turbulent stream, the ability to compute bulk quantities such as the sediment flux in rivers remains poor. For instance, the sediment flow rates measured in gravel-bed rivers differ within one to two orders of magnitude from the bed-load transport equations (Wilcock 2001; Martin 2003; Barry et al. 2004). In order to better understand the physical processes ruling bed-load solid transport at the grain scale, an experimental study of the motion of coarse spherical glass beads entrained by a turbulent and supercritical water flow down a steep channel with a mobile bed was set up. The initial width was 6.5 mm slightly larger than the particle diameter of 6 mm to create a two-dimensional particle flow allowing recording from the side all particles with a high speed camera. The overall aim of this research is to measure the trajectories of all particles and to analyze the fluctuations of the solid discharge as well as the state of movement (rolling or saltation). First the trajectory of a single saltating or rolling particle was analyzed (Ancey et al. 2002; Ancey et al. 2003). Secondly, the aim was to measure the trajectories of all particles and to analyze the fluctuations of the solid discharge as well as the state of movement, rolling or saltation (Boehm et al. 2004; Boehm 2005; Boehm et al. 2006). More recently a doubled width of 12.7 mm was also investigated. The objective of this paper is to present data focusing on global time-averaged hydrodynamic and bed load results. Results will first be discussed for each width taking account of wall effects. Non-dimensioned solid discharge vs. Shields numbers will be analyzed and compared with classical formulae.

2 EXPERIMENTAL FACILITIES AND TECHNIQUES

2.1 *Channel*

Experiments were carried out in a tilted, narrow, glass-sided channel, 2 m in length. Figure 1 shows a sketch of the experimental facility. The channel width W was initially adjusted to 6.5 mm, which was slightly larger than the particle diameter (6 mm). In this way, the particle motion was approximately two-dimensional and stayed in the focal plane of the camera. The channel slope $\tan\theta$ ranged from 7.5% to 15% (i.e., channel representative of steep gravel-bed rivers as

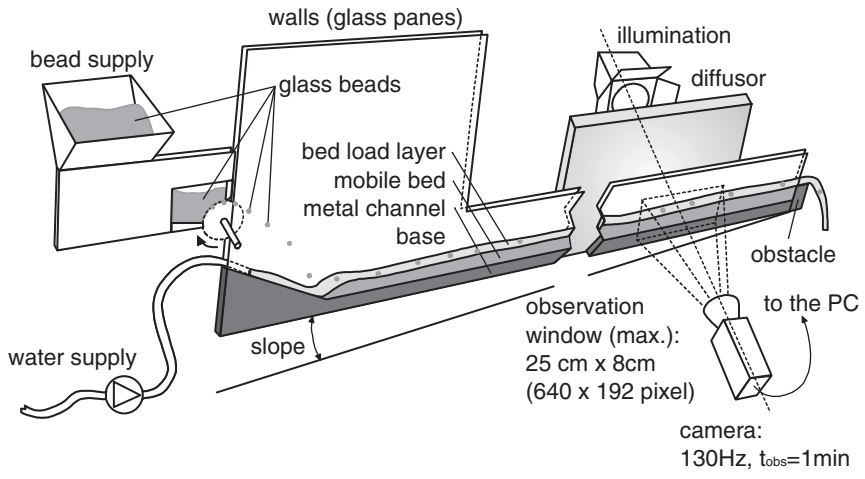

Figure 1. Sketch of the experimental setup.

Table 1. Flow characteristics and time-averaged values of dimensionless numbers characterizing bed load and water flow for width 6.5 mm. Varying parameters: Channel inclination $\tan\theta$ and solid discharge $\dot{n}$. The notation E7-6 indicates: $\tan\theta \approx 7\%$ and $\dot{n} \approx 6$ beads/s. Not all experiments made at $\tan\theta = 10\%$ are reported here, see (Boehm et al. 2004; Boehm 2005) for further information.

Experiment	E7-6	E7-8	E7-9	E10-16	E12-9	E12-16	E12-21	E15-16	E15-21
$\tan\theta$ (%)	7.5	7.5	7.5	10	12.5	12.5	12.5	15.0	15.0
$\dot{n}$ (beads/s)	5.7	7.8	8.7	15.4	9.3	15.2	20.0	15.6	21.5
q_w (10^{-3} m^2/s)	10.00	11.54	13.85	8.19	2.97	3.85	4.46	2.31	2.92
C_s (%)	0.95	1.17	1.16	3.30	5.58	7.02	7.74	11.65	12.23
h (mm)	18.9	20.8	24.9	16.9	7.0	8.2	9.4	4.9	6.7
u_f (m/s)	0.53	0.55	0.56	0.48	0.42	0.47	0.48	0.47	0.44
Re	5860	6230	6400	5280	3760	4360	4600	3680	3830
Fr	1.26	1.26	1.15	1.24	2.20	2.09	1.90	3.72	2.63
h/d	3.16	3.47	4.15	2.82	1.17	1.37	1.56	0.82	1.11
$2h/W$	5.83	6.40	7.65	5.21	2.16	2.53	2.88	1.51	2.05

encountered in mountain areas). In order to test the influence of the channel slope on bed load, 15 experiments with different inclinations and various flow rates (see Table 1) were first set up. The channel base consisted of half-cylinders of equal size ($r = 3$ mm), but they were randomly arranged on different levels, from 0 to 5.5 mm, by increments of 0.5 mm. These levels were generated using a sequence of uniformly distributed random numbers. Disorder was essential as it prevented slipping of entire layers of particles on the upper bed surface, which would have induced artificial erosion conditions. Maintaining disorder in monosized spherical particles is difficult, with severe constraints (Bideau and Hansen 1993), here involving mainly how to create disorder in the packing and the bed thickness. For thick beds (typically, whose thickness exceeded 5–6 particle diameters), a regular, crystalline arrangement was observed along the upper part of the bed. This is expected since it is well-known that the disorder range induced by a defect in a crystalline arrangement of monosized spherical particles is a few particle diameters (Bideau and Hansen 1993). Therefore, in order to be able to control the order in the particle arrangement, we built beds whose thicknesses did not exceed 5 particle diameters. The effects of disorder on bed-load transport features have been presented in another paper (Boehm et al. 2004). An obstacle was set at the channel outlet to enable bed formation and prevent full bed erosion; its height could be adjusted.

More recently, 33 new experiments were performed with a width of 12.7 mm about two bead diameters

Table 2. Flow characteristics and time-averaged values of dimensionless numbers characterizing bed load and water flow at a width of 12.7 mm. Varying parameters: Channel inclination $\tan\theta$ and solid discharge $\dot{n}$. The notation F7-8 indicates: $\tan\theta \approx 7\%$ and $\dot{n} \approx 8$ beads/s. See (Dufresne 2005) for further information.

Experiment	F7-8 to F7-26	F10-8 to F10-25	F12-11 to F12-19	F15-19 and F15-24
$\tan\theta$ (%)	7.5	10	12.5	15
$\dot{n}$ (beads/s)	8.4–25.6	8.2–25.3	11.4–19.4	19.0–24.4
q_w (10^{-3} m^2/s)	5.91–11.50	3.86–6.86	3.13–3.60	2.70–3.06
C_S (%)	1.2–1.7	1.9–3.8	3.2–4.8	6.3–7.1
h (*mm*)	13.7–26.2	9.4–14.3	9.1–11.4	10.4–10.5
u_f (m/s)	0.43–0.60	0.37–0.51	0.30–0.37	0.26–0.29
Re	7490–12210	5850–7540	4800–5600	4080–4630
Fr	1.17–1.34	1.06–1.39	0.91–1.22	0.81–0.92
h/d	2.3–4.3	1.6–2.4	1.5–1.9	1.7–1.8
$2h/W$	2.2–4.1	1.5–2.2	1.4–1.8	1.6–1.7

(see Table 2). In that case, there is no more problems in creating disorder as there is an added widthwise degree of freedom. The first objective was to adapt the image analysis algorithms preparing for studying two-size mixtures. the second objective whose results are reported in this paper was to assess the influence of the width and wall effects of this unusually narrow channel.

2.2 *Solid and water supplies*

Black spherical glass beads with a nominal diameter d of 6 mm and a density ρ_p of 2500 kg/m^3 (provided by Sigmund Lindner GmbH, Germany) were used. They were injected from a reservoir into the channel using a wheel driven by a direct current motor and equipped with 20 hollows on the circumference, as depicted in figure 1. For the experiments presented here, the injection rate $\dot{n}$ ranged from 5 to 26 beads per second, with an uncertainty of less than 5%. This corresponded to a volumic solid discharge per unit width q_s of $7 - 38 \times 10^{-5}$ m^2/s. The water supply at the channel entrance was controlled by an electromagnetic flow meter provided by Krohne (France). The discharge per unit width q_w ranged from 3 to 15×10^{-3} m^2/s. The values for 6.5 mm wide runs (labelled E) are summarized in Table 1 and ranges of values for 12.7 mm wide runs (labelled F) appear in Table 2.

2.3 *Dimensionless numbers*

The hydraulic conditions can be specified using classic dimensionless numbers. In tables 1 and 2, h is the time-averaged flow depth. To make the particle rate $\dot{n}$ more palpable, we express it in beads/s instead of m^3/s. The flow Reynolds number is defined as $\mathrm{Re} = 4R_h\bar{u}_f/\nu$, where $R_h = Wh/(2h+W)$ denotes hydraulic radius, $\bar{u}_f = q_w/h$ fluid velocity (averaged in the y- and z-directions), ν kinematic viscosity of water. The Froude number $\mathrm{Fr} = \bar{u}_f/\sqrt{gh}$ (where g denotes gravity acceleration) varied significantly over the experiment duration and along the main stream direction. The mean Fr values are reported.

The Shields number is defined as the ratio of the bottom shear stress ($\tau_0 = \rho_p g R_h \tan\theta$) to the stress equivalent of the buoyant force of a particle lying on the bottom (Julien 1994): $\tau* = \tau_0/(gd(\rho_p - \rho_f))$. The solid concentration is defined as the ratio of the solid and the water discharge $C_s = q_s/q_w$. The ratio h/d is low, typically in the range 0.8–4. A few aspects of the free-surface line and the bed configuration are shown in the tabulated figure 2 for the experiments in the 6.5 mm wide channel. Figure 3 shows a typical image obtained in the 12.7 *mm* wide channel compared to an image at a width of 6.5 *mm* where trajectories of all beads are two-dimensional. Disorder induced by the doubled width appears quite obviously.

Note that the dimensionless number values differ substantially from the values usually found in the hydraulics literature. The reason is twofold: first we used a short and narrow channel, which led to studying low Reynolds number regimes, whereas in most experiments on bed load transport, one takes care to avoid such regimes; this is the price to pay to have access to the details of particle movements. Since we used coarse particles, particle motion was weakly dependent on the actual value of the flow Reynolds number and turbulence structure. Therefore we think that the small size of the experimental setup is not a handicap. Second we mostly studied supercritical flows because of the steep slopes investigated. However, in a supercritical regime, flow depth was low: on the order of the particle size, meaning that particle motion was affected by the water free surface.

2.4 *Experimental procedures*

The preliminary procedure can be split into three major steps. First of all, a particle bed was built along the

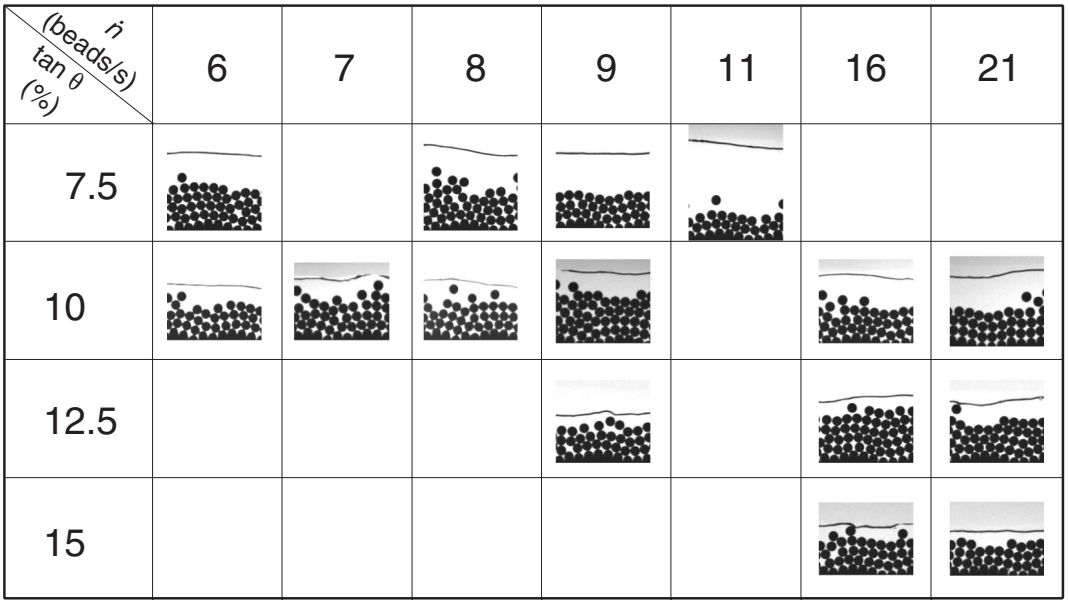

Figure 2. Overview of the experiments conducted for width 6.5 mm at various solid discharges $\dot{n}$ and slopes $\tan\theta$. For each experiment, a detail of one filmed image is shown. See Table 1 for the experimental conditions.

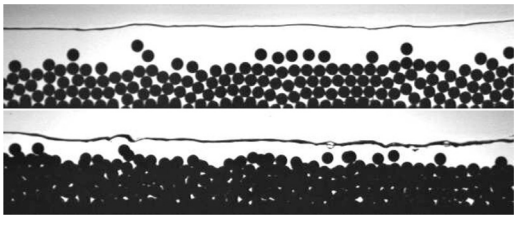

Figure 3. Typical images obtained respectively in the 6.5 *mm* (above) and 12.7 *mm* (below) wide channel.

channel base, which remained stationary on average. To that end, an equilibrium between the water discharge, solid discharge, bed elevation, and channel slope was sought. This equilibrium was reached by using the following procedure:

1. The water discharge q_w was set to a constant value.
2. An obstacle (approximately 20 mm in height) was positioned at the downstream end of the channel. The solid discharge $\dot{n}$ at the channel entrance was set to a constant value. The solid discharge per unit width q_s was calculated by the relation $q_s = \pi d^3 \dot{n}/(6W)$. The first beads supplied by the feeding system were stopped by the obstacle at the channel outlet and started to form a bed. The bed line rose to the level of the obstacle and beads began to leave the channel. After approximately 10 minutes, the system arrived at bed load equilibrium, i.e., there was no more bed deposition or erosion over a sufficiently long time interval.
3. In order to make the bed line parallel with the channel base, the water discharge was then adjusted. After several iterations, we arrived at the configuration of a bed that consisted of two to three almost stationary bead layers along the channel, for which the bed line slope matched the channel base inclination. Average equilibrium conditions were sustained over long time periods, basically as long as 30 minutes.

Once bed equilibrium was reached, the particles and the water stream were filmed using a Pulnix partial scan video camera (progressive scan TM-6705AN). The camera was placed perpendicular to the glass panes at a distance of 115 cm from the channel, approximately 80 cm upstream from the channel outlet. It was inclined at the same angle as the channel. Lights were positioned in the backside of the channel. An area of approximately 25 cm in length and 8 cm in height was filmed and later reduced to accelerate image processing.

The camera resolution was 640×192 pixels for a frame rate of $f = 129.2$ fps (exposure time: 0.2 ms, 256 gray levels). Each sequence was limited to 8000 images due to limited computer memory; this corresponded to an observation duration of approximately 1 minute.

Each experiment was repeated at least twice in order to spot possible experimental problems and to get an idea of the data scattering.

2.5 *Image and data processing*

Images were analyzed using the WIMA software, provided by the *Traitement du Signal et Instrumentation* laboratory in Saint-Etienne (France). Positions of the bead mass centers were detected by means of an algorithm combining several image-processing operations. It compared the filmed images with the image of a model bead and calculated the correlation maxima to obtain the bead positions. Data obtained from the image sequences were analyzed to obtain the particle trajectories. For this purpose, we developed a particle-tracking algorithm. This algorithm compared the bead positions of two consecutive images to determine the trajectory of each bead step by step. Since the particle movement was nearly two-dimensional and the displacement of a particle between two images was always smaller than a particle diameter, the trajectories (approximately 700 per sequence) could be calculated with no significant error. The state of movement of a particle was also defined by considering that each bead was always either in a resting, rolling, or saltating regime (Boehm et al. 2006; Boehm 2005). In this paper image analysis was only used to measure the water depth. Since the experiments involved a mobile bed, the water depth was defined as the difference between the free surface and the bed surface elevation. The water free surface (averaged in the direction perpendicular to the channel walls) was detected using its slim form; missing portions were inter- or extrapolated. For the 6.5 mm width the bed surface profile was taken as the line linking the top points of the uppermost resting or rolling beads. For the width 12.7 mm, a different algorithm was used to derive the bed line combining derivative and morphological operators (Dufresne 2005).

3 RESULTS

3.1 *Analysis of uncorrected data*

A widespread way of representing bed load transport rates for different flow conditions is to plot the dimensionless solid discharge ϕ as a function of the Shields number $\tau*$. The solid discharge was made dimensionless by the definition

$$\phi = q_s/\sqrt{(\rho_p/\rho_f - 1)gd^3},$$

where q_s is the bed load transport rate per unit width, $q_s = \pi d^3 \dot{n}/6W$.

First, the Shields number $\tau*$ was calculated with the global hydraulic radius.

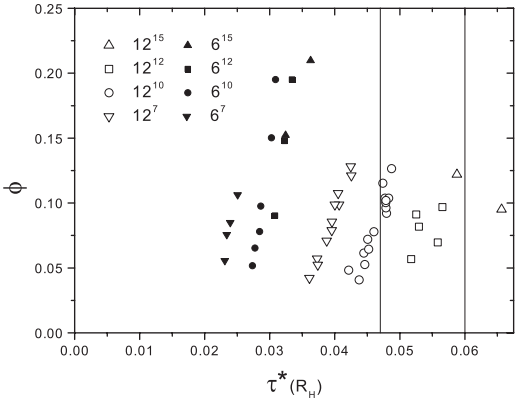

Figure 4. Relations between dimensionless solid discharges and uncorrected Shields numbers. Black lines correspond to incipient motion thresholds: $\tau* = 0.06$ or $\tau* = 0.047$.

Although the dimensionless solid discharge increases with the Shields number on figure 4, most of the values of Shields number are lower than widely accepted incipient motion thresholds ($\tau* = 0.06$ or $\tau* = 0.047$). Moreover experiments at width 6.5 mm and 12.7 mm are separated in two groups and it seems that data are scattered depending on the slope value. A closer look on data within tables shows that the lowest values of $\tau*$ are obtained for the highest values of the aspect ratio $2h/W$. This behavior is then clearly due to side-wall effects.

3.2 *Side-wall correction procedure*

The purpose of this section is to present the method used to calculate a bottom hydraulic radius. The method used is the well-known Einstein's method (Cao 1985).

This method is based on three hypotheses:

- three Darcy–Weisbach equations can be written:

$$\sqrt{\frac{8}{f}} = \frac{u_f}{\sqrt{gR_h sin\theta}} \tag{1}$$

$$\sqrt{\frac{8}{f_b}} = \frac{u_f}{\sqrt{gR_{h_b} sin\theta}} \tag{2}$$

$$\sqrt{\frac{8}{f_w}} = \frac{u_f}{\sqrt{gR_{h_w} sin\theta}} \tag{3}$$

- the energy slope is the same for each area,
- the flow velocity is the same for each area.

With theses hypotheses, we can write the following equations:

$$\frac{f}{R_h} = \frac{f_b}{R_{hb}} = \frac{f_w}{R_{hw}} \tag{4}$$

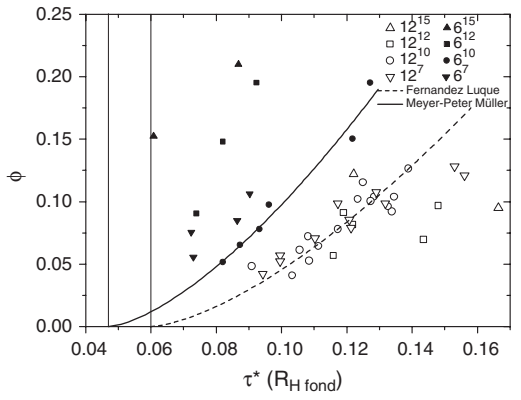

Figure 5. Relations between dimensionless solid discharges and Shields number calculated with the bottom hydraulic radius. Black lines correspond to incipient motion thresholds: $\tau* = 0.06$ or $\tau* = 0.047$.

$$\frac{Re}{f} = \frac{Re_b}{f_b} = \frac{Re_w}{f_w} \tag{5}$$

$$f_b = f + \frac{2h}{W}(f - f_w) \tag{6}$$

f_w is calculated with the following turbulent and smooth formula (Graf and Altinakar 1993):

$$\frac{1}{\sqrt{f_w}} = 2log(Re_w\sqrt{f_w}/4) + 0.32 \tag{7}$$

f_b is then calculated by using *eq.* 6 and knowing f and $2h/W$. R_{h_b} is calculated with the help of eq 4.

It must be stressed that the Einstein's method is usually applied to account for minor side-wall effects. In our case, the $2h/W$ ratio is always above 1 meaning that the water depth is always superior to the width. The side-wall effects are then important and it can be questioned whether the Einstein's method would be relevant in our case. Results are presented on figure 5. By comparing with figure 4, we can see that results are relevant with incipient motion thresholds because all points are above these levels. We notice too that the two groups of points (width 6.5 mm and width 12.7 mm) are nearer than on figure 4. Although more than a mild correction the Einstein's method proved in our case relatively efficient in so far as corrected data appear to agree with classical results.

In addition both the two widely used Meyer-Peter Müller (Meyer-Peter and Muller 1948) and Fernandez Luque semi-empirical formulae (Fernandez Luque and van Beek 1976) are plotted on figure 5. Note that these empirical formulas were established for slopes much lower than in our case, but this should not be a major issue since the physics should remain essentially the same.

Our data lie relatively near incipient motion as our maximum Shields Number is only about three times critical incipient motion Shields Numbers. Although it is well known that empirical formulae do not perform well near the threshold of motion, our data, most surprisingly, relatively agree with those formulae which again shows that the Einstein's method is relevant. A closer look to figure 5 reveals that data for the steepest slopes (12.5% and 15%) agree the least with the formulae. As already discussed, at the lower width, these data have the lowest h/d submergence ratio approaching 1 which means that the free surface acts as a physical barrier truncating the saltation trajectories and forcing most particles to move in the rolling regime. As the saltation of a single particle has been used as a theoretical basis to establish semiempirical bed-load formulae (Bagnold 1973; Wiberg and Smith 1985; Wiberg and Smith 1989; Bridge and Bennett 1992), it is not surprising that those formulae are not in good agreement with data presenting the lowest h/d ratios (Ancey et al. 2005).

4 CONCLUSIONS

In this paper, global time-averaged hydrodynamic and bed load results obtained on an idealized very narrow channel are presented. This channel was primarily designed for studying bed load from a physical viewpoint at the grain scale, the width of the channel being the same as the particle diameter. To analyze results from the fluid mechanics viewpoint and to study the wall effects, a double width was investigated. Nondimensional bed load solid discharges vs. uncorrected Shields numbers appeared quite scattered depending on width and slope but more precisely on the aspect ratio. The classical use of the Einstein's method to account for side-wall effects proved efficient although in our case hypotheses behind this method could be questionable. Corrected results were in good agreement with classical incipient motion Shields numbers and compared favorably with two specific semiempirical bed-load formulae. For steeper slopes with low submergence of the order of the particle diameter more deviation was observed probably because the assumptions underlying the classical bed load formulae do not hold any more.

The experimental set-up was designed to be as simple as possible to gain access to the trajectories of all particles for studying solid discharges fluctuations and motion regimes. In particular analysis of probability distribution functions are thought to help better modelling of bed-load especially near incipient motion. However the crucial question is whether upscaling from the grain scale to the reach scale would be possible with results obtained in this narrow channel. The global results presented in this paper are encouraging

in that perspective. The use of the simple Einstein's correction to account for side-wall effects appears enough to yield results comparable to data obtained with classical large tilting flumes and natural materials. In short, our experimental set-up makes it possible to bridge the gap between the physics and the fluid mechanics approaches in bed load research.

ACKNOWLEDGMENTS

This study was supported by the program ECCO/PNRH of INSU and ANR. We are grateful to the laboratory TSI UMR 5516 of University of Saint Etienne, France (Christophe Ducottet, Nathalie Bochard, Jacques Jay, and Jean-Paul Schon).

REFERENCES

Ancey, C., F. Bigillon, P. Frey, and R. Ducret (2003). Rolling motion of a bead in a rapid water stream. *Phys. Rev. E 67*, 011303.

Ancey, C., F. Bigillon, P. Frey, R. Ducret, and J. Lanier (2002). Saltating motion of a bead in a rapid water stream. *Phys. Rev. E 66*, 036306.

Ancey, C., T. Boehm, P. Frey, M. Jodeau, and J.-L. Reboud (2005). Saltating or rolling stones? In *River coastal and estuarine morphodynamics 2005*, Urbana-Champaign, USA, pp. 641–651. AIRH.

Bagnold, R. (1973). The nature of saltation and of 'bed load' transport in water. *Proc. Roy. Soc. London A 332*, 473–504.

Barry, J., J. Buffington, and J. King (2004). A general power equation for predicting bed load transport rates in gravel bed rivers. *Water Resour. Res. 40*, W10401.

Bideau, D. and A. Hansen (Eds.) (1993). *Disorder and granular media*. Random materials and processes. Amsterdam: North-Holland.

Boehm, T. (2005). *Motion and interaction of a set of particles in a supercritical flow*. Ph. D. thesis, Joseph Fourier University, Grenoble.

Boehm, T., C. Ancey, P. Frey, J.-L. Reboud, and C. Duccotet (2004). Fluctuations of the solid discharge of gravity-driven particle flows in a turbulent stream. *Phys. Rev. E 69*, 061307.

Boehm, T., P. Frey, C. Ducottet, C. Ancey, M. Jodeau, and J.-L. Reboud (2006). Two-dimensional motion of a set of particles in a free surface flow with image processing. *Experiments in Fluids, in press*.

Bridge, J. and S. Bennett (1992). A model for the entrainment and transport of sediment grains of mixed sizes, shapes, and densities. *Water Resour. Res. 28*, 337–363.

Cao, H. (1985). *résistance hydraulique d'un lit de gravier mobile a pente raide; étude éxperimentale*. Ph. D. thesis, Ecole Polytechnique Federale de Lausanne.

Dufresne, M. (2005). Etude exprimentale du transport de particules solides par charriage a forte pente. Master's thesis, Louis Pasteur University, ENGEES, Strasbourg.

Fernandez Luque, R. and R. van Beek (1976). Erosion and transport of bed-load sediment. *J. Hydraul. Res. 14*, 127–144.

Graf, W. and M. Altinakar (1993). *Hydraulique fluviale*, Volume 2. Lausanne: Presses polytechniques et universitaires romandes.

Julien, P.-Y. (1994). *Erosion and Sedimentation*. Cambridge: Cambridge University Press.

Martin, Y. (2003). Evaluation of bed load transport formulae using field evidence from the Vedder River, British Columbia. *Geomorphology 53*, 75–95.

Meyer-Peter, E. and R. Muller (1948). Formulas for bed load transport. In IAHR (Ed.), *2nd meeting*, Stockholm.

Wiberg, P. and J. Smith (1985). A theoretical model for saltating grains in water. *Journal of Geophysical Research (C4) 90*, 7341–7354.

Wiberg, P. and J. Smith (1989). Model for calculating bedload transport of sediment. *J. Hydraul. Eng. 115*, 101–123.

Wilcock, P. (2001). Toward a practical method for estimating sediment-transport rates in gravel bed-rivers. *Earth Surface Processes and Landforms 26*, 1395–1408.